

Summary of the Structure Functions Working group at DIS 2012

Amanda Cooper-Sarkar¹, Pedro Jimenez-Delgado², Ringailė Plačakytė³,

¹Denys Wilkinson Bdg, Keble Rd, OX1 3RH OXFORD, UK

²Institut für Theoretische Physik, Universität Zürich, 8057 Zürich, Switzerland
Jefferson Lab, 12000 Jefferson Avenue, Newport News, VA 23606, USA

³DESY, Notkestraße 85, 22607 Hamburg, Germany

DOI: will be assigned

A summary of the recent experimental, phenomenological and theoretical results presented in the Structure Functions working group at DIS2012 workshop.

1 Introduction

In the Structure Functions working group experimental results relevant to the determination of parton distributions were presented by H1, ZEUS, ATLAS, CMS and LHCb. The HERAFitter tool, which is an open access code for fitting PDFs to relevant data, and an update of the FastNLO tool, which allows the fast computation of higher-order cross sections at hadron colliders, were presented. Progress in the determination of the parton distributions of the nucleon from most global PDF groups was reviewed and more restricted studies which focus on particular aspects of these determinations were also discussed. Analyses of nuclear PDFs were presented. Finally, phenomenological contributions within frameworks which appear as extensions or alternatives to the usual collinear factorization approach were discussed.

2 Summary of the presentations

A measurement of the integrated luminosity of HERA data collected in the years 2003 to 2007 and based on the elastic QED Compton process $ep \rightarrow e\gamma p$ has been performed by the H1 Collaboration [1]. Contrary to the standard HERA luminosity measurement which exploits Bethe-Heitler (BH) scattering with electron and the photon emitted almost collinearly to the incident electron, the particles in QED Compton scattering have a sizable transverse momentum with respect to the incident electron and are detectable in the main H1 detector. The advantage of this method is its insensitivity to the details of the beam optics, but its disadvantage is limited statistical precision. The precision of the experimental and theory uncertainties in this analysis are illustrated using the variable $(E - p_z)/(2E_e^0)$ in Fig. 1. This variable is calculated from the sum of the four-momenta of the electron and the photon (where E_e^0 is electron beam energy) and is expected to peak at unity. The tail to small values of $(Ep_z)/(2E_e^0)$ originates from initial state radiation (where theory uncertainty dominates), whereas values larger than unity occur

due to resolution effects. The measured integrated luminosity is determined with a precision of 2.3% and is in agreement with the Bethe-Heitler measurement which has larger uncertainty for the second period of HERA data taking.

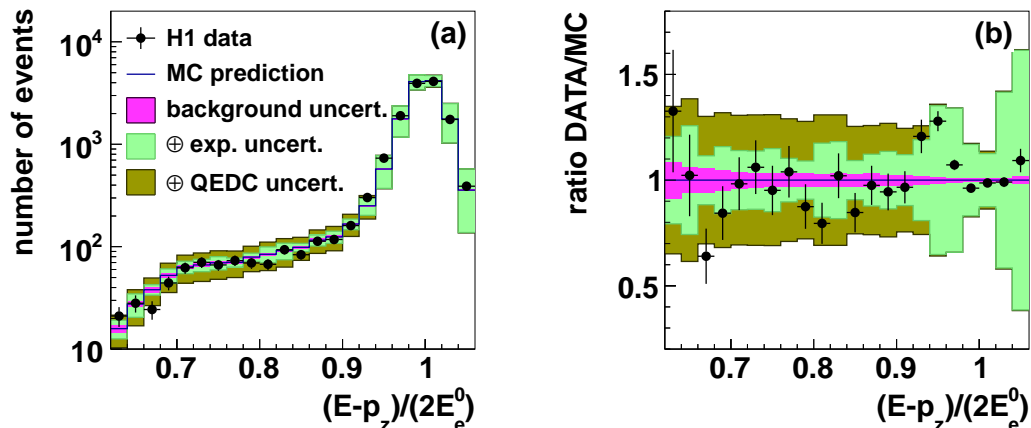


Figure 1: Distribution of the variable $(Ep_z)/(2E_e^0)$ (see text) calculated from the sum of the electron and photon four-momenta. In (a) the event counts are shown and in (b) the ratio of data to expectation is drawn. The data are shown as black dots with the statistical uncertainties indicated as vertical bars and the simulation (including background) is indicated as a solid line, with various components of the systematic uncertainty shown as shaded areas.

ZEUS have completed the measurement of inclusive cross sections from HERA-II running by finalising the Neutral Current (NC) e^+p measurement [2]. The measurements are based on an integrated luminosity of 135.5 pb⁻¹ taken in 2006 and 2007 at a centre-of-mass energy of 318 GeV. The double-differential cross sections in Q^2 and x have been measured in the kinematic region $Q^2 > 185$ GeV² for both positively and negatively polarised positron beams. These measurements have been used to extract the polarisation asymmetry parameter $A^+ = \frac{2}{(P_+ - P_-)} \frac{(\sigma^+(P_+) - \sigma^+(P_-))}{(\sigma^+(P_+) + \sigma^+(P_-))}$, where $P_+ = +0.32$ and $P_- = -0.36$ denote the magnitude of the beam polarisations and $\sigma^+(P)$ denotes the cross section measured at polarisation P . This quantity is sensitive to the electro-weak vector couplings of the quarks and the non-zero asymmetry observed is a direct measure of parity violation. The NC e^+p data may also be averaged over positive and negative polarisations and combined with 169.9 pb⁻¹ of NC e^-p measurements [4] to yield the structure function xF_3 , which gives information on valence parton distribution functions. The measurement of xF_3 as a function of x in Q^2 bins is shown in Fig. 2, compared to predictions from HERAPDF1.5

The H1 and ZEUS experiments have already combined their data from HERA-I running [5] and have made preliminary combinations of HERA-II data from nominal energy and low energy running. A preliminary combination of $F_2^{c\bar{c}}$ data has also been made. These combined data sets, together with data on inclusive jet production from both H1 and ZEUS, have been used as the input to extract parton distribution functions (PDFs) in the HERAPDF1.7 NLO QCD fit [6]. These PDFs are illustrated in Fig. 2. All of the input data sets are well fit and consistent. In comparison to the published HERAPDF1.0 PDFs [5], which were based only on the HERA-I

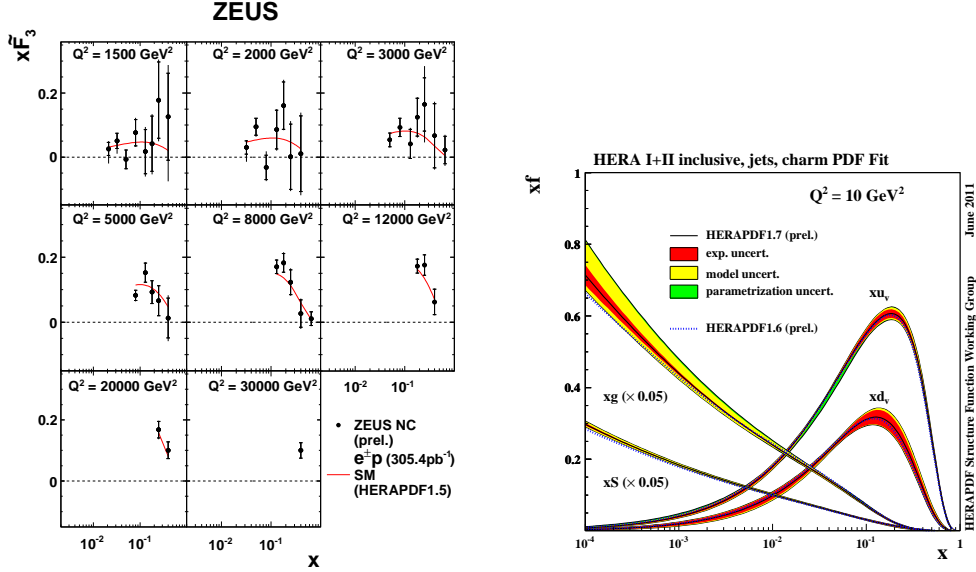


Figure 2: Left: the structure function xF_3 as a function of x in Q^2 bins, compared to the predictions of HERAPDF1.5. Right: Parton distribution functions for HERAPDF1.7

combination, the HERA-II high Q^2 cross-sections further constrain the high- x valence PDFs; the HERA-II low energy runs help to constrain the low- x gluon PDF; the charm data constrain heavy quark schemes and the jet data help to constrain $\alpha_s(M_Z)$.

Using jet production data in PDF fitting requires fast repeated computation of NLO jet cross sections. The FastNLO [7] package provides a method to store the matrix elements calculated for such higher-order cross-sections on grids such that the cross-sections may be calculated quickly by convolution of these grids with the input PDFs. The package can be used for jet cross-sections from DIS and from hadron colliders. Typical applications of FastNLO are data and theory comparisons for various PDF sets, derivation of scale uncertainties, determination of α_s . Fig 3 shows the comparison of the inclusive jet data from various experiments to theory predictions obtained with FastNLO. Version 2 of the FastNLO project offers variety of new features for users including largely improved technical aspects of the code (like improved reading tools) and flexibility in e.g. scale composition or scale variation. More details about new features in the version 2 of the FastNLO can be found in [8].

The HERAFitter tool has been developed by H1 and ZEUS as an open access code for fitting PDFs to relevant data [9]. Whereas the HERAFitter has been developed from the HERAPDF QCD fitting framework, based on QCDNUM for the NLO and NNLO QCD evolution, it goes far beyond this. The package can be used to fit all types of data used in a global PDF fit: inclusive cross sections, heavy quark structure functions, jet production data from Deep Inelastic Scattering (DIS); inclusive cross-section from fixed target data; Drell-Yan (including W, Z) cross sections from fixed target data and from Tevatron and LHC data; jet cross-sections from Tevatron and LHC data. A variety of options which facilitate benchmarking are available with the package: experimental systematic uncertainties can be treated as correlated or uncorrelated

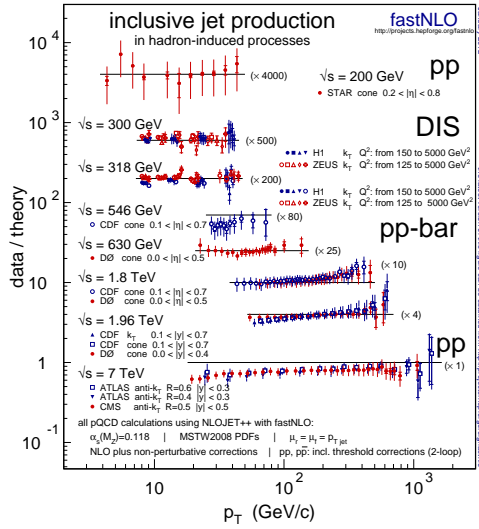


Figure 3: An overview of data over theory ratios for inclusive jet cross sections, measured in different processes at different center-of-mass energies. The data are compared to calculations obtained by FastNLO. The inner error bars represent the statistical errors and the outer error bars correspond to the quadratic sum of all experimental uncertainties.

and PDF uncertainties may be evaluated from the Hessian covariance matrix or by the generation of Monte-Carlo replicas; the structure functions may be computed in a variety of heavy quark schemes; the package is interfaced to both FastNLO and to Applgrid for the fast and correct input of NLO jet cross sections and Drell-Yan cross sections and the input of top cross sections via HATHOR is under development. Plotting tools are provided for the fit output and the resulting PDFs are supplied in the LHAPDF format. The package is under continuous development to provide a common platform for useful tools; for example the NNPDF reweighting tool has been included to allow fast computation of the impact of new data on existing PDFs, and the package has recently been extended to make fits to diffractive cross sections and to make fits using dipole models.

CMS has measured differential jet cross sections using $\sqrt{s} = 7$ TeV data corresponding to 4.6 pb⁻¹ of 2010 data [10]. Reconstructed jets in this measurement cover rapidity up to $|y| = 2.5$, transverse momentum up to $p_T = 2$ TeV and dijet invariant mass up to $M_{JJ} = 5$ TeV. The measured cross sections are compared to perturbative QCD predictions at next-to-leading order using various sets of PDFs. Fig 4 illustrates the inclusive jet cross sections together with theoretical predictions obtained using the central value of the NNPDF set (left) and ratio of these cross sections to the NNPDF prediction with predictions from other PDF sets also shown (right). Experimental and theoretical uncertainties in the measurement are comparable in size so that these data should be able to constrain PDF uncertainties. The systematic uncertainty correlations which are necessary for the PDF fits are in preparation.

ATLAS has made a measurement of inclusive jet production using 36 pb⁻¹ of data from 2010 running [11]. The data are provided with full information on correlated systematic uncertainties and this allows them to have some constraining power on PDFs. These data are well fit by most modern PDF sets such as MSTW08, CT10, NNPDF2.1 and HERAPDF1.5, however they prefer a somewhat less hard high- x gluon than the Tevatron jet data. Fig. 5 shows a comparison of these data to current PDFs. Dijet data from 4.7fb⁻¹ of 2011 data are also available [11] extending the range of the di-jet mass to 4.8 TeV. These data are also illustrated in Fig. 5.

ATLAS have presented W -lepton and Z differential cross sections. as a function of (pseudo-

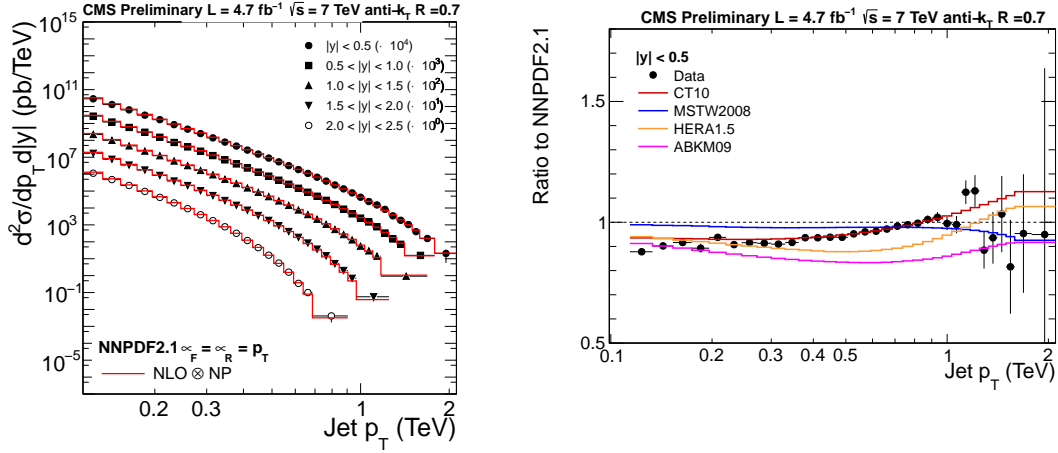


Figure 4: Inclusive jet cross sections (left) and ratio of inclusive jet (right) measured at CMS compared to theoretical prediction using the central value of the NNPDF PDF set. The solid histograms in the ratio plot also show expectations obtained with other PDF sets.

)rapidity and as a function of p_t from 36pb^{-1} of 2010 data. The Z rapidity distribution from combined electron and muon decay channels is shown in Fig. 6. Data is also available in the τ decay channels and measurements of W and τ polarisation have been made [12]. The W, Z rapidity distributions are supplied with full information on correlated systematic uncertainties and this allows them to have impact on PDF fits. In particular, in Fig. 6 the Z rapidity data are presented compared to two PDF fits done using these ATLAS W^\pm and Z data together with the HERA DIS data. The fit labelled 'epWZ fixed \bar{s} ' has the strange quark density suppressed and fixed to 50% of the down sea quark density at the starting scale of PDF evolution $Q_0^2 \sim 2 \text{ GeV}^2$ (as suggested by neutrino di-muon data). The fit labelled 'epWZ free \bar{s} ' allows the strange quark distribution freedom in normalisation and shape, with the result that ATLAS data clearly prefer unsuppressed strangeness for $x \sim 0.01$ [13]. Fig. 6 compares the ratio of the strange to down sea quark densities at $x = 0.023$, $Q_0^2 = 1.9 \text{ GeV}^2$, from the preferred epWZ free \bar{s} fit to that of other PDF determinations.

Measurements of Z or W boson production associated with heavy quarks in the final state can provide important information about heavy quark densities in PDFs. The process $pp \rightarrow W + c + X$ and the cross section ratios $R_{+/-} = \sigma(W^+ c + X)/\sigma(W^- c + X)$ and $R_c = \sigma(W + c + X)/\sigma(W + jets + X)$ measured at CMS [14] provide information about the strange and anti-strange quark parton density functions of the proton. In these measurements muonic decays of the W -boson and lifetime tagging techniques are used to extract the charm fraction in $W + jet$ events. The measured ratios are: $R_{+/-} = 0.92 \pm 0.19(stat.) \pm 0.04(syst.)$ and $R_c = 0.143 \pm 0.015(stat.) \pm 0.024(syst.)$. Currently the 20% total uncertainty of these results limits their constraining power but higher statistics samples will significantly improve the sensitivity to the strangeness content of the PDFs. Results on the production of b jets in association with Z/γ^* were also presented by CMS collaboration [14].

The LHCb experiment has also performed measurements of W and Z production using final states containing muons, electrons and tau leptons [15]. The LHCb data provide unique constraints on both low- x and high- x PDFs because of the high pseudorapidity region ($\eta > 2.5$)

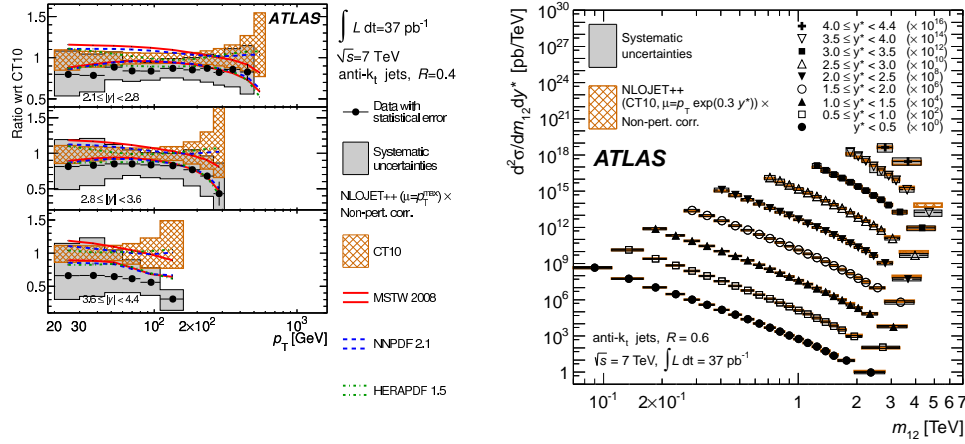


Figure 5: Left: ATLAS data on inclusive jet cross sections as a function of p_t in high rapidity bins. The data are shown in ratio to the predictions of NLOjet++ made using CT10 PDFs, with other PDF predictions shown for comparison. Right: ATLAS di-jet data as a function of di-jet invariant mass in rapidity bins

in which the W and Z boson cross sections are measured. Differential cross sections, W and Z cross section ratios and the lepton charge asymmetry are measured in this kinematic region. Fig. 7 shows the W -lepton asymmetry at high rapidity. The results presented use mainly 2010 data such that they are still limited by statistical precision and the uncertainty on the luminosity. Precision is expected to improve significantly with the full 2011 dataset.

LHCb have also performed the first low mass Drell-Yan cross section measurements [16] for which theoretical uncertainties (particularly scale uncertainties) and PDF uncertainties are larger compare to W and Z measurements. Differential DY cross sections are measured as a function of dimuon invariant mass (starting from 5 GeV, see Fig 7) and as a function of rapidity. This preliminary result uses background template technique [16] and currently is limited in statistical and systematic precision. Significantly smaller uncertainties in the measurement reaching even lower masses are expected with 2011 data set where luminosity is about 30 times higher.

The NNPDF collaboration have examined the impact of the LHC data on PDF fits but the early LHC data which was included in the NNPDF2.2 set are now superceded. At this meeting a preliminary examination of the impact of more recent LHC data on the NNPDF fit was presented [17]. This includes the ATLAS 2010 W -lepton and Z rapidity distributions, the higher luminosity CMS W -lepton asymmetry measurements, the LHCb Z and W -lepton high rapidity distributions, and the ATLAS and CMS inclusive jet measurements. The impact of these data has been evaluated by the technique of PDF reweighting. Of all these data sets the most discriminating is the ATLAS W^\pm -lepton and Z data. Their discriminating power is such that of 1000 initial Monte-Carlo replicas form NNPDF2.1 only 16 survive the reweighting procedure. Fig. 8 shows the impact of these data on the down quark PDF shape and uncertainty. Such a large change necessitates a fresh PDF fit which is underway.

The latest ABM11 PDF analysis [19] uses an improved treatment of heavy quark electro-

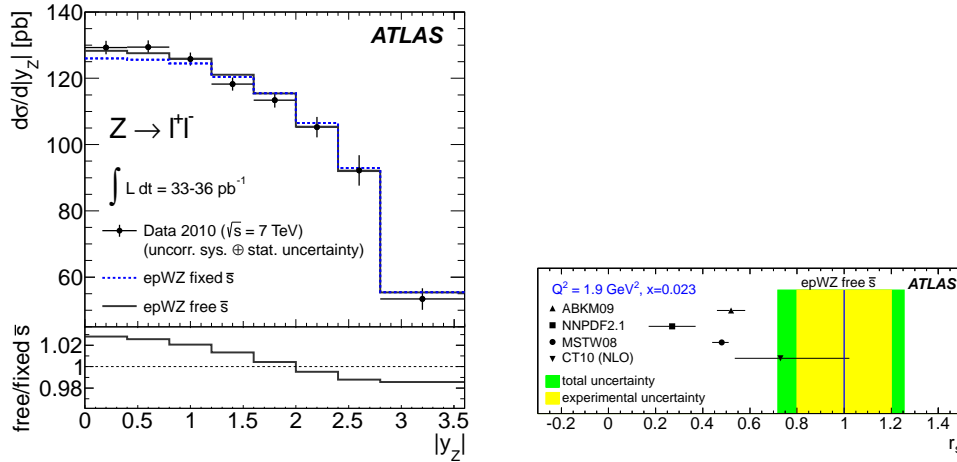


Figure 6: Left: ATLAS data on the Z rapidity distribution from combined electron and muon data. The data are compared to two PDF fits, one with fixed suppressed strangeness and the other with free unsuppressed strangeness as described in the text. Right: the ratio of strange to down quark densities in the sea, at $x = 0.023$, $Q^2 = 1.9\text{GeV}^2$, from the preferred epWZ free \bar{s} fit and from other PDF determinations.

production within the fixed-flavor-number scheme at NNLO. This includes the $\overline{\text{MS}}$ scheme for heavy quark masses. They find good agreement with the latest (combined) HERA charged current data, in particular no indication of *large logs* up to high Q^2 . The discriminating power of current F_L measurements in the small x region is shown in Fig. 9. A similar situation is pointed out for dimuon production data. The ABM determination of $\alpha_s(M_Z^2)$ is lower than that reported by MSTW and/or NNPDF. It is often suggested that this is because jet data are not included in the ABM fit. However ABM find good agreement with jet data. They suggest that the higher values found by other groups could originate in higher twist effects in the fixed target DIS data. Such power corrections are explicitly included in the ABM formalism.

The ongoing update of the NNLO *dynamical* parton distributions was presented[20]. This includes several improvements in the framework, e.g. a more careful determination of the strange-quark input parton distributions, a complete treatment of the correlations of systematic uncertainties of the data, and an improved treatment for heavy quark electroproduction from [19]; a wealth of deuteron DIS data which were not included in the JR09 analysis is also a major update. Nevertheless, there are only moderated changes of 10% or less with respect to JR09. In particular, the value of $\alpha_s(M_Z^2)$ is determined to be $\sim 0.113 \rightarrow 0.114$, depending on the value of the input scale used; the difference between these values is regarded as a genuine uncertainty of the determination [21].

The CTEQ collaboration has also presented their NNLO results [22]. There are two different sets at NNLO, one based on pre-LHC data only (CT10) and one which will include LHC data on W and Z rapidity distributions (CT12). There are ongoing investigations on the flavor structure of the quark sea at $x < 10^{-2}$; in particular the possibility of $\bar{d} \neq \bar{u}$ as $x \rightarrow 0$, as well as the relative size of the strange-quark distribution. Benchmark cross-sections at NNLO are presented for the first time.

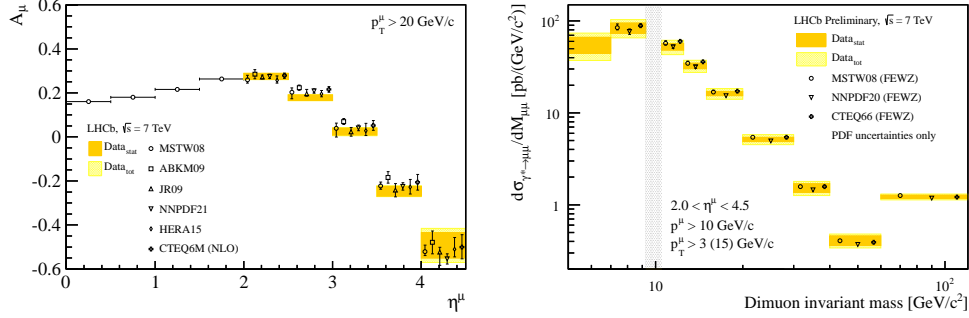


Figure 7: Left: Lepton charge asymmetry A_μ in bins of muon pseudorapidity where dark shaded bands correspond to the statistical (dark shaded/orange) and systematic (light hatched/yellow) experimental uncertainties. These are compared to NNLO and NLO predictions with different PDF sets shown by symbols with error bars where the PDF and the theoretical uncertainties are added in quadrature. Right: Differential DY cross section as a function of the dimuon invariant mass. Measurements are compared to theoretical predictions calculated with FEWZ using different PDF sets.

The CTEQ-JLab Collaboration (CJ) [23] focus on the determination of PDFs in the large- x region, with the aim of using the unique capabilities of the CEBAF accelerator to measure small cross sections at extreme kinematics to reduce the large PDFs uncertainties at large x . This requires a careful account of corrections which are sometimes suppressed by kinematic cuts in other analyses, e.g. higher-twist terms, target mass corrections, nuclear corrections, etc. The current focus is on different nuclear corrections in NLO predictions for parton distributions and structure functions.

A very careful re-analysis of non-singlet world data on unpolarized structure functions in the valence region was presented in ref. [24]. NLO, NNLO and even approximate N³LO expressions are used in the valence region to precisely extract the value of the strong coupling constant $\alpha_s(M_Z^2)$ and the higher twist contributions. The contributions of twist $\tau = 3$ and higher to the polarized structure functions $g_1(x, Q^2)$ and $g_2(x, Q^2)$ are also investigated. At NNLO the value $\alpha_s(M_Z^2) = 0.1132 \pm 0.0022$ is obtained in good agreement with other determinations [19, 20].

An alternative approach to PDFs is based on the statistical model in which the nucleon is regarded as a gas of massless partons in equilibrium at a given temperature in a volume of finite size. Only 9 free parameters are adjusted in order to completely determine the unpolarized and polarized (helicity) distributions. This model produces a reasonable qualitative description, even for some data which were not included in the fits. Updates to include more recent data in the framework are under consideration.

Before the year 2000 prompt photon data had been used as a means of constraining the gluon distribution. However, it was dropped due to discrepancies between some of the fixed target data sets and theoretical predictions. There has recently been a suggestion to re-instate prompt photon data [18] using only high hadron collider data, which agree well with predictions made using JETPHOX. The impact of these data on the NNPDF2.1 fit has been evaluated by PDF reweighting and the data have some impact on the gluon distribution at $x \sim 0.01$, as illustrated in Fig. 8

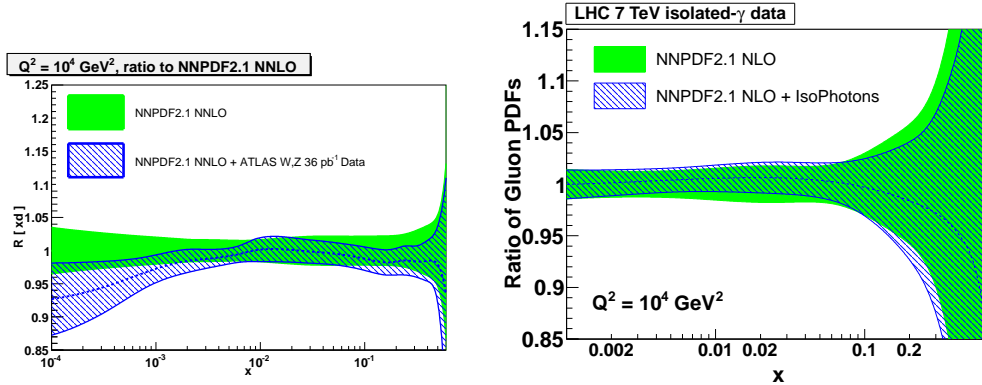


Figure 8: Left: The ratio of the NNPDF2.1 down quark PDF before and after reweighting to include the ATLAS W, Z data, including uncertainties. Right: The ratio of the NNPDF2.1 gluon PDFs before and after reweighting to include prompt photon data, including uncertainties

The nCTEQ group reported [26] difficulties in describing simultaneously the commonly used charged-lepton DIS and Drell–Yan dilepton production off nuclear targets, and data on neutrino-nuclei scattering. The source of the problem involves the data/error estimates of the NuTeV neutrino data for which the correlations of systematic errors need to be taken into account. This is in contrast to the results presented in [27], where a consistent picture of universal nuclear modification factors was reported. They find it possible to describe the main features of all nuclear data, including neutrino DIS as well as inclusive pion production, without finding any significant tension among the different data sets.

An analysis of HERA data on the proton structure function F_2 in the low- x regime using BFKL evolution was presented in ref. [28]. A NLL framework which includes running coupling effects and makes use of collinear improved resummation is used to achieve a good description of the data and to study theoretical uncertainties.

The process $W/Z/DY + \text{jet}$, where the boson is produced in the forward direction of one of the colliding protons and the jet is produced in the forward direction of the second proton, has been proposed for searches of evidence for BFKL evolution [29]. First numerical results for a number of observables which allow the isolation of BFKL effects were presented.

Another contribution within the BFKL framework was the calculation of the next-to-leading order photon impact factor for small- x DIS [30]. An analytic expression in momentum space is derived using the operator product expansion in Wilson lines.

The CCFM unintegrated PDF for the gluon has been determined [31] using the combined HERA data. For a good description of HERA data a calculation of the gluon splitting function including non-singular terms, imposition of kinematic constraints and an NLO treatment of α_s are all necessary. The analysis has been supplemented with an error estimation which allows the study of the uPDF uncertainty for processes at HERA and LHC.

Extensions of the CCFM evolution equations have been studied [32] with the aim of addressing effects like parton saturation in final states at the LHC. The question of how to combine the physics of the BK and CCFM evolution equations has been investigated and a possible non-linear extension of the CCFM equation has been obtained, as suggested by an exclusive form of the BK equation.

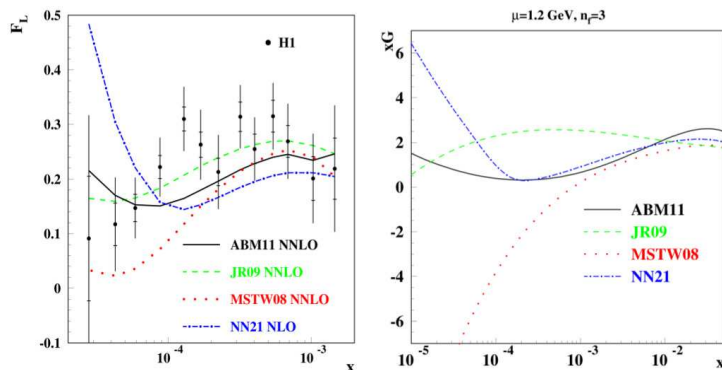


Figure 9: Discriminating power of current F_L data between different gluons at small x [19].

General bounds on the ratio of structure functions F_L/F_2 have been derived within the dipole picture [33], which are valid for any dipole cross-section and sharpened by including information on the charm structure function F_2^c . The bounds are respected by the data within the experimental errors, although for $3.5 \text{ GeV}^2 \leq Q^2 \leq 20 \text{ GeV}^2$ the central values of the data are close to (and in some cases even above) the bounds, and thus put some strain on the validity of the dipole model.

An effort to understand the small- x behavior of the structure function F_2 on general grounds was presented [34]. It is shown that studies in field theory indicate that this behavior may be described as a *critical* phenomenon. Under the assumption of a simple power law behavior of the matrix elements in the scattering region one can derive an expression for F_2 which depends on some critical indices which should be calculable using lattice methods. A phenomenological extraction of these coefficients lead to values similar to those obtained with a two pomeron fit.

3 Conclusion

The Structure Functions session at DIS2012 was very lively with many new experimental results, especially from the LHC on Drell-Yan production, including W and Z , and on jet production, including jets with heavy flavours. There has been substantial progress in the development of tools for parton fitting. The determinations of parton distribution functions from different groups still give rise to some controversy but there is progress in understanding the differences and progress in refining the calculations which go into these analyses. All groups now present PDFs up to NNLO in the DGLAP formalism. The analysis of nuclear PDFs is coming of age. There has also been progress in calculations which extend this formalism into the BFKL regime and the high-density regime.

Acknowledgements

We thank the organisers for the invitation to convene this session and we thank all the speakers in our session for their contributions and the lively discussions. This research is

supported in part by the Swiss National Science Foundation (SNF) under contract 200020-138206. Authored by Jefferson Science Associates, LLC under U.S. DOE Contract No. DE-AC05-06OR23177. The U.S. Government retains a non-exclusive, paid-up, irrevocable, world-wide license to publish or reproduce this manuscript for U.S. Government purposes.

4 Bibliography

References

- [1] **H1** Collaboration, F.D. Aaron et al, hep-ex/1205.2448, 2012.
- [2] F. Januszek, these proceedings;
<https://indico.cern.ch/contributionDisplay.py?sessionId=8&contribId=34&confId=153252>
- [3] **H1 and ZEUS** Collaborations, V. Radescu, Pos ICHEP2010(2010)168
- [4] **ZEUS** Collaboration, S. Chekanov et al, EPJC62(2009)625
- [5] F.D. Aaron et al, JHEP1001(2010)109.
- [6] K. Nowak, these proceedings;
<https://indico.cern.ch/contributionDisplay.py?sessionId=8&contribId=35&confId=153252>
- [7] T. Kluge, K. Rabbertz, M. Wobisch, "FastNLO: Fast pQCD Calculations for PDF Fits".
hep-ph/0609285v2.
- [8] D. Britzger, these proceedings;
<https://indico.cern.ch/contributionDisplay.py?sessionId=25&contribId=165&confId=153252>
- [9] V. Radescu, these proceedings;
<https://indico.cern.ch/contributionDisplay.py?sessionId=8&contribId=344&confId=153252>
- [10] O. Kaya, these proceedings;
<https://indico.cern.ch/contributionDisplay.py?sessionId=25&contribId=312&confId=153252>
- [11] B. Malaescu, these proceedings;
<https://indico.cern.ch/contributionDisplay.py?sessionId=25&contribId=71&confId=153252>
- [12] J.P. Sauvan, these proceedings;
<https://indico.cern.ch/contributionDisplay.py?sessionId=23&contribId=76&confId=153252>
- [13] U. Klein, these proceedings;
<https://indico.cern.ch/contributionDisplay.py?sessionId=8&contribId=297&confId=153252>
- [14] M. Musich, these proceedings;
<https://indico.cern.ch/contributionDisplay.py?sessionId=23&contribId=229&confId=153252>
- [15] S. Farry, these proceedings;
<https://indico.cern.ch/contributionDisplay.py?sessionId=23&contribId=147&confId=153252>
- [16] J. Anderson, these proceedings;
<https://indico.cern.ch/contributionDisplay.py?sessionId=23&contribId=145&confId=153252>
- [17] M. Ubiali, these proceedings;
<https://indico.cern.ch/contributionDisplay.py?sessionId=8&contribId=300&confId=153252>
- [18] D. d'Enterria and J. Rojo, Nulc.Phys.B860(2012)311.
- [19] S. Alekhin, these proceedings;
<https://indico.cern.ch/contributionDisplay.py?sessionId=8&contribId=302&confId=153252>
- [20] P. Jimenez-Delgado, these proceedings;
<https://indico.cern.ch/contributionDisplay.py?sessionId=8&contribId=299&confId=153252>
- [21] Pedro Jimenez-Delgado, arXiv:1206.4262 [hep-ph].
- [22] P. Nadolsky, these proceedings;
<https://indico.cern.ch/contributionDisplay.py?sessionId=8&contribId=301&confId=153252>

- [23] C. Keppel, these proceedings;
<https://indico.cern.ch/contributionDisplay.py?sessionId=8&contribId=290&confId=153252>
- [24] J. Blümlein, these proceedings;
<https://indico.cern.ch/contributionDisplay.py?sessionId=8&contribId=303&confId=153252>
- [25] F. Buccella, these proceedings;
<https://indico.cern.ch/contributionDisplay.py?sessionId=8&contribId=95&confId=153252>
- [26] K. Kovarik, these proceedings;
<https://indico.cern.ch/contributionDisplay.py?sessionId=8&contribId=155&confId=153252>
- [27] R. Sassot, these proceedings;
<https://indico.cern.ch/contributionDisplay.py?sessionId=8&contribId=33&confId=153252>
- [28] C. Salas, these proceedings;
<https://indico.cern.ch/contributionDisplay.py?sessionId=8&contribId=97&confId=153252>
- [29] M. Hentschinski, these proceedings;
<https://indico.cern.ch/contributionDisplay.py?sessionId=23&contribId=115&confId=153252>
- [30] G. A. Chirilli, these proceedings;
<https://indico.cern.ch/contributionDisplay.py?sessionId=8&contribId=128&confId=153252>
- [31] H. Jung, these proceedings;
<https://indico.cern.ch/contributionDisplay.py?sessionId=8&contribId=29&confId=153252>
- [32] K. Kutak, these proceedings;
<https://indico.cern.ch/contributionDisplay.py?sessionId=8&contribId=31&confId=153252>
- [33] C. Ewerz, these proceedings;
<https://indico.cern.ch/contributionDisplay.py?sessionId=8&contribId=159&confId=153252>
- [34] O. Nachtmann, these proceedings;
<https://indico.cern.ch/contributionDisplay.py?sessionId=8&contribId=118&confId=153252>

ZEUS

